







Article

$K_d(\text{PAR})$ and a Depth Based Model to Estimate the Height of Submerged Aquatic Vegetation in an Oligotrophic Reservoir: A Case Study at Nova Avanhandava

Luiz Henrique Rotta ^{1,*} , Deepak R. Mishra ² , Enner Alcântara ³ , Nilton Imai ¹ ,
Fernanda Watanabe ¹  and Thanan Rodrigues ⁴ 

¹ Department of Cartography—Presidente Prudente, São Paulo State University (UNESP), São Paulo, SP 19160-900, Brazil; nilton.imai@unesp.br (N.I.); fernanda.watanabe@unesp.br (F.W.)

² Department of Geography, University of Georgia (UGA), Athens, GA 30609, USA; dmishra@uga.edu

³ Department of Environmental Engineering—São José dos Campos, São Paulo State University (UNESP), São Paulo, SP 12245-000, Brazil; enner.alcantara@unesp.br

⁴ Federal Institute of Education, Science and Technology of Pará State (IFPA), Castanhal, PA 68740-970, Brazil; thanan.rodrigues@ifpa.edu.br

* Correspondence: lh.rotta@unesp.br; Tel.: +55-18-3229-5500

Received: 11 December 2018; Accepted: 29 January 2019; Published: 5 February 2019



Abstract: Submerged aquatic vegetation (SAV) carry out important biological functions in freshwater systems, however, uncontrolled growth can lead to many negative ecologic and economic impacts. Radiation availability is the primary limiting factor for SAV and it is a function of water transparency measured by $K_d(\text{PAR})$ (downwelling attenuation coefficient of Photosynthetically Active Radiation) and depth. The aim of this study was to develop a $K_d(\text{PAR})$ and depth based model to estimate the height of submerged aquatic vegetation in a tropical oligotrophic reservoir. This work proposed a new graphical model to represent the SAV height in relation to $K_d(\text{PAR})$ and depth. Based on the visual analysis of the model, it was possible to establish a set of Boolean rules to classify the SAV height and identify regions where SAV can grow with greater or lesser vigor. $K_d(\text{PAR})$ was estimated using a model based on satellite data. Overall, the occurrence and height of SAV were directly influenced by the $K_d(\text{PAR})$, depending on the depth. This study highlights the importance of optical parameters in examining the occurrence and status of SAV in Brazilian Reservoirs. It was concluded that the digital model and its graphical representation overcomes the limitations found by other researchers to understand the SAV behavior in relation to those independent variables: depth and $K_d(\text{PAR})$.

Keywords: remote sensing; water quality; inland waters; Boolean classification; echosounder data

1. Introduction

Reservoirs are constructed for many purposes, including flood prevention, irrigation, navigation, functioning as a drinking water supply, fishing, recreation and power generation. According to Wetzel [1], reservoirs are intermediate systems between rivers and natural lakes in terms of their morphology, hydrology, nutrient loadings and cycling, and sources of organic matter. They are similar to dynamic lakes; however, a significant portion of their volume has the characteristics and biological functions of a river [1]. The main primary producers in reservoirs are the same as found in rivers and lakes: phytoplankton, photoautotrophic bacteria, periphytic algae, and floating, submerged or fixed rooted macrophytes [2].

Submerged aquatic vegetation (SAV) is vital in maintaining biodiversity in reservoirs, lakes and other freshwater systems because of their numerous functions such as influencing nutrient cycling,

maintaining water and sediment chemistry, providing food and shelter, and increasing the habitat complexity [3]. On the other hand, unregulated growth of SAV can lead to many negative ecologic and economic impacts on reservoir functions affecting water-based navigation, the water quality and supply, power generation, irrigation, fisheries, recreation, human and animal health, and land values [4,5]. The primary productivity of SAV is limited by several factors such as temperature, radiation availability, stream velocity, water level variation, nutrient concentration, competition for space, and inorganic carbon [6–8]. However, radiation availability is the main limiting factor for submerged aquatic macrophytes [9–16].

The most reliable estimate of the light requirement by SAV can be determined by comparing in situ depth distribution of SAV with the diffuse attenuation coefficient of downwelling irradiance (K_d) [17]. K_d controls the propagation of light through water [14]. It is possible to quantify the presence of light in different depths by using K_d estimates and determining the depth of the euphotic zone [18,19], which in turn controls the presence or absence of SAV [15,16].

Several biophysical characteristics of the SAV can be related to light availability. Havens [10] studied SAV biomass and their relationship with environmental variables in Lake Okeechobee (USA) and observed that the low SAV biomass may be due to the influence of suspended solids on underwater irradiance field, as well as the high water level. Similarly, the biomass and the maximum depth of macrophytes colonization were studied by Hudon et al. [20] in the St. Lawrence River and Ottawa River (Canada). They concluded that the maximum depth of SAV colonization could be predicted from the light extinction coefficient (K), calculated as the slope of the natural log transformed values of light penetration at increasing depth (I_z), divided by surface light intensity (I_0). The total biomass of macrophytes was related to the exposure to wind and waves, plant growth forms, water depth, and light intensity.

Vestergaard and Sand-Jensen [21] examined the relationship between environmental factors and the richness of the submerged macrophytes in Danish lakes (Denmark). The mean species richness increased significantly with increasing transparency. Depth limits for growth of eelgrass (*Zostera marina*) and macroalgae increased linearly with the transparency in Danish coastal waters [22]. An inverse relationship between SAV height and attenuation of photosynthetic active radiation ($K_{d(PAR)}$) was observed in a study by Rotta et al. [15]. The study found that the locations with high transparency (low $K_{d(PAR)}$) in the Nova Avanhandava Reservoir (Brazil) favored the development of tall SAV compared to areas with high $K_{d(PAR)}$.

It is known that the radiation availability for the SAV growth is a function of (a) water transparency, efficiently measured by $K_{d(PAR)}$, and (b) depth, since the greater the depth, the lower the radiation availability. The submerged relief (bathymetry) is usually known in the Brazilian reservoirs, and the K_d can be estimated by using existing empirical algorithms or quasi-analytical algorithms (QAA) based on multispectral images such as OLI/Landsat-8 and MSI/Sentinel-2 [23–26]. Despite this, there is no simple way to classify regions with a greater chance of finding taller SAV. In other words, there is still no easy and fast solution to produce a map showing the spatial distribution of SAV heights in a reservoir; such information would be highly valuable for the management of aquatic vegetation in reservoirs.

Some questions still remain when one examines the effect of the water column depth and $K_{d(PAR)}$ on the SAV height, such as, in the high transparency (or low transparency) condition, what is the influence of depth on the SAV height? At a given depth, what is the relationship between $K_{d(PAR)}$ and the SAV height? In which situations does one variable stand out from the other? In short, how does one associate depth and attenuation to predict where SAV can grow with greater or lesser vigor? SAV height, $K_{d(PAR)}$ and spatial distributions of water depth, usually represented in a spatial database as layers, not showing the relationship among them, hampering information acquisition about the SAV quantity. This work proposes a new graphical model to represent the SAV height in relation to $K_{d(PAR)}$ and depth, aiming at answering the questions raised before and, then, provide relevant information about the SAV in the reservoir. The main objective is to classify the region, where transparency

and water depth are combined making them ideal for SAV growth. The specific objectives were (i) to estimate the $K_d(\text{PAR})$ using a model based on satellite imagery; and (ii) to investigate the spatial distribution of SAV height and depth based on echosounder data acquired in the field.

2. Materials and Methods

2.1. Study Area

The study was conducted in a section of the Nova Avanhandava Reservoir, indicated with the red dashed rectangle in Figure 1. Nova Avanhandava Reservoir is located in the cascading system of the Tietê River, in São Paulo State, Brazil. Nova Avanhandava located in Buritama city started its operation in 1982. The concrete dam is 2038 m in length. It has a flooded area of 210 km² and volume of 2.8×10^9 m³. The region's economy is primarily based on agriculture and cattle farming, with significant acreage covering sugarcane crop [27]. This reservoir is used mainly for hydropower generation, transportation of agricultural products, irrigation, fishing and public and industrial provisioning [28]

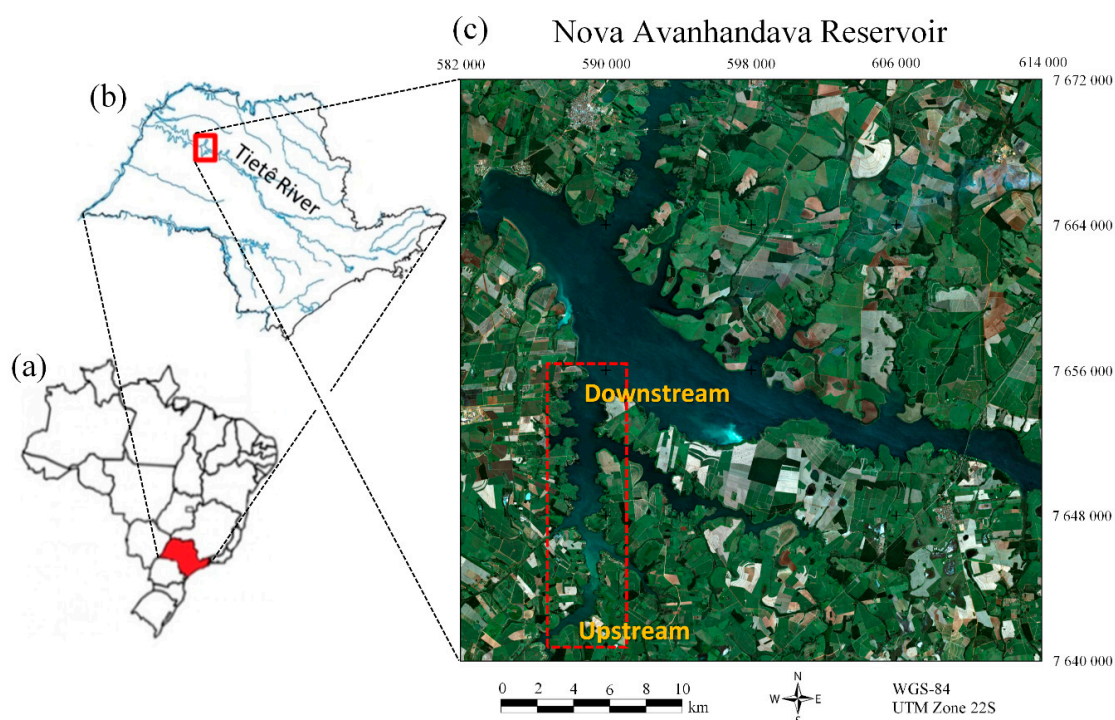


Figure 1. The study area in (a) Brazil and (b) the São Paulo state. (c) Nova Avanhandava Reservoir and the actual research site indicated with the dashed red rectangle (Bonito River). Downstream and upstream regions are indicated in (c). Image: SPOT- 6 bands 2, 1, 0 as RGB (July 9th, 2013; WGS-84; UTM Zone 22S).

Nova Avanhandava is a run-of-river reservoir. Therefore, the water level changes within any given year are not significant. A study conducted by Cavenaghi et al. [29] in Nova Avanhandava reservoir showed that the SAVs of greater importance are *Egeria densa* and *Egeria najas*. Based on the field campaign, *Egeria* spp. was predominant in the entire studied area (Bonito River) and TSS (Total Suspended Solids) of 0.5–3.9 mg L⁻¹ and Chl-*a* (Chlorophyll-*a* concentration) of 3.0–19.8 µg L⁻¹ were observed. The study of SAV in Nova Avanhandava can bring important contributions since the growth of this kind of vegetation can either benefit or damage the reservoir's operation. According to Velini et al. [30], aquatic vegetation can be necessary as a source of O₂, food and shelter for aquatic life, however, large masses of these macrophytes can make navigation, fishing, and recreation harder, and can obstruct turbine water inlets in hydroelectric power plants.

2.2. Field Campaign and Data Analysis

The data were acquired in two field campaigns. The first campaign was held between June 28th and 30th and the second on July 4th and 5th 2013. The field campaigns were chosen based on the local weather when cloud cover was low. The optical data collected in the first campaign were used to calculate the remote sensing reflectance (R_{rs}) and diffuse the attenuation coefficient of PAR ($K_d(\text{PAR})$). In the second field campaign, the echosounder data were collected to measure the depth and SAV height in the study area.

2.2.1. Optical Data

TriOS/RAMSES (ACC-VIS and ARC-VIS) optical sensors (<http://www.trios.de>; Rastede, Germany) were used in the field campaign to measure the downwelling irradiance (E_d) and upwelling radiance (L_u). Both hyperspectral UV/VIS irradiance and radiance sensors have 190 channels between 320 and 950 nm, and a spectral sampling of 3.3 nm with a wavelength accuracy of 0.3 nm. Hyperspectral E_d data were collected at various depth intervals, $E_d(Z)$, in the water column up to about 1% of $E_d(0-)$ (downwelling irradiance just below the water surface), at 10 sampling stations in optically deep water, i.e., regions with reflectance without a bottom signal, as shown in Figure 2.

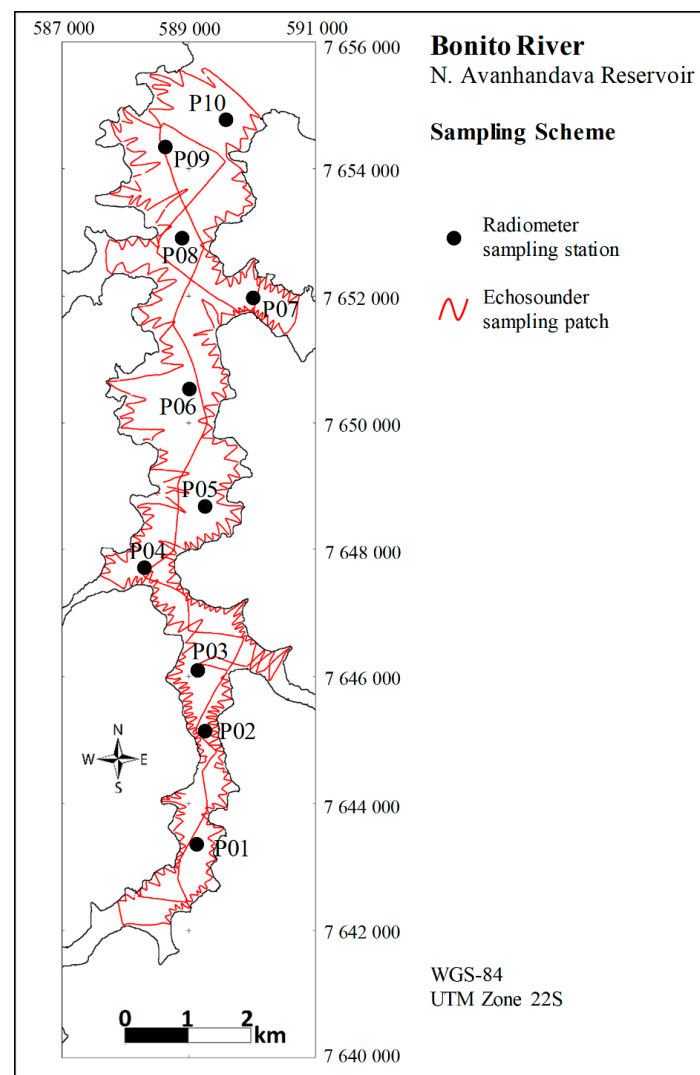


Figure 2. The optical data sampling stations (black dots) in Bonito River and echosounder sampling transects (red lines).

R_{rs} was calculated using the upwelling radiance just below-surface ($L_u(\lambda)(0^-)$) and downwelling irradiance above-surface ($E_d(\lambda)$), based on Dall'olmo and Gitelson [31] and Gitelson et al. [32]:

$$R_{rs}(\lambda) = \frac{L_u(\lambda)}{E_d(\lambda)} \frac{t}{n^2} F_i \quad (1)$$

where, t is the transmittance at air-water interface (0.98), n is the refractive index of water relative to air (1.33), and F_i is the spectral immersion coefficient (λ dependent) (~ 1.7). To predict the $R_{rs}(\lambda)$ signal that would be recorded by the satellite sensor at each channel centered at wavelength λ , weighted averages of each R_{rs} spectrum were calculated by using the spectral band responses of SPOT-6 as weights [33]:

$$R_{rs}^{SPOT}(\lambda) = \frac{\sum_{\lambda} R_{rs}(\lambda) \times S(\lambda)}{\sum_{\lambda} S(\lambda)} \quad (2)$$

where, $S(\lambda)$ is the SPOT-6 spectral response function, and $R_{rs}^{SPOT}(\lambda)$ is the predicted R_{rs} .

According to Kirk [14], photosynthetic pigments absorb light energy from the underwater light field in the visible spectrum from 400 to 700 nm range (Photosynthetically Active Radiation (PAR)). E_d of PAR ($E_{d(PAR)}$) was estimated by integrating the E_d ranging from 400 to 700 nm. $K_{d(PAR)}$ was estimated based on Mobley [34]:

$$E_{d(PAR)}(Z) = E_{d(PAR)}(0^-) e^{-K_{d(PAR)} Z} \quad (3)$$

where, $E_{d(PAR)}(Z)$ is the $E_{d(PAR)}$ at depth Z , $E_{d(PAR)}(0^-)$ is the $E_{d(PAR)}$ just below the surface, and Z is depth.

$K_{d(PAR)}$ can be derived as:

$$K_{d(PAR)} = \frac{\ln E_{d(PAR)}(0^-) - \ln E_{d(PAR)}(Z)}{Z} \quad (4)$$

2.2.2. Echosounder Data

Hydroacoustic measurements were collected by a DT-X scientific echosounder (<http://www.biosonicsinc.com/>; Biosonics, Seattle, WA, USA) and used to acquire the SAV height, depth and position data at study area, between July 4th and 5th, 2013. Echosounder data recorded in numerous transects were represented as red lines in Figure 2. The echosounder data were visualized and recorded in real time via a laptop using the *Visual Acquisition* software, Biosonics [35], which displays an echogram with the depth and SAV height. The sensor emits 10 acoustic pulses per second. The stored data were processed through the *EcoSAV* software, Biosonics [36]. Each set of 10 pulses yields a line in an ASCII file that contains the day, hour, position (lat., long.), depth (m), coverage (%), and mean height of the SAV. The echosounder data were collected considering an appropriate spatial distribution, with more than 15,000 sample points in the entire study area. The echosounder was calibrated as per the Biosonics recommendations [37] using a standard target sphere of known target strength (TS). The echosounder data was not compared with actual in situ measurement of SAV, because the Biosonics DT-X sensor and software have been evaluated in other studies. Sabol et al. [38] used divers to measure the distance between the transducer face, top of the SAV canopy, and the bottom. Close agreement between true SAV height and the hydroacoustic estimates was found, with R^2 of 0.78. Chamberlain et al. [39] also found similar agreement between ground-truth and hydroacoustic datasets.

2.3. $K_d(PAR)$ Mapping

SPOT-6 image is comprised of bands B0 (455–525 nm), B1 (530–590 nm), B2 (625–695 nm) and B3 (760–890 nm). The predicted SPOT-6 bands ($R_{rs}^{SPOT}(\lambda)$) were used for the $K_{d(PAR)}$ model calibration. Linear regressions were tested between $K_{d(PAR)}$ and $R_{rs}^{SPOT}(\lambda)$ (visible bands). The best model was

selected based on the coefficient of determination (R^2) and the Root-Mean-Square-Error (RMSE) [26]. Due to the low number of samples for model calibration, the Leave-One-Out Cross Validation (LOOCV) method was used to evaluate the models, so that it was not necessary to split samples for validation. In LOOCV, the model is calibrated using all data with the exception of one point, then the mean squared error is computed based on this point [40,41]. The $K_{d(PAR)}$ model was applied to the atmospherically corrected SPOT-6 image producing a thematic map.

The SPOT image was acquired for the Nova Avanhandava Reservoir at 13:08:43 (GMT) on July 9th, 2013 across an angle of -6.6002° and along an angle of 19.1336° , in WGS-84 coordinate system. The atmospheric correction of SPOT-6 image was performed using FLAASH - an atmospheric correction tool based on MODTRAN4 (MODerate spectral resolution atmospheric TRANsmittance algorithm and a computer model) [42]. Parameters to characterize the atmospheric conditions and illumination/viewing geometry at the time of image acquisition were incorporated in FLAASH. Others input parameters were set as follows: initial visibility of 70 km, sensor altitude of 695 km, ground elevation of 362 m, zenith angle of 161.5° and azimuth angle of 195° .

2.4. Depth and SAV Height Mapping

Depth and SAV height data acquired by echosounder were interpolated using the Kriging method. Kriging is a geostatistical interpolator aiming to determine the spatial distribution and variability of a variable [43]. Echosounder data were recorded in numerous transects according to red lines in Figure 2. All the 23×10^3 sample points were used for interpolation. Kriging interpolation of SAV distribution can produce better predictions when compared with other non-geostatistical interpolations [44,45].

The anisotropy was checked based on the semivariogram in a different direction for each dataset. A spatial phenomenon is considered anisotropic when its pattern of variability changes according to the direction variation [46]. After confirming the anisotropy, the direction of the greater range or variability was found. Semivariograms were calculated varying the direction in 45° based on the greater range or sill and with a tolerance of 22.5° . The size of the angular window for the experimental variogram is defined by the tolerance. The tolerance of 22.5° was selected to ensure that the data analyzed in one direction are not contained in the data analyzed in another direction. Since SAV growth mostly occurs along the margins, the greater range on SAV height will occur in the same direction of the river flow, that is, approximately 70° (with the North direction being 90°). It is known that the depth increases from the margin to the thalweg. Thus, greater variability in the 0° direction was expected.

After its calculation, the experimental semivariograms must be fitted with any variogram, such as linear, exponential, circular, etc. [46,47]. In this work, we used the exponential model for interpolating the depth and SAV height. Finally, the anisotropy ratio and anisotropy angle based on the direction of greater range or sill was defined. The fitted model based on the semivariogram was used in data interpolation. The grid of each variable generated from the kriging method was sliced into different thematic classes. Classes with intervals of 0.2 m for the SAV map were used. A last thematic class greater than 2 m was established, since there were a few occurrences of SAV values taller than 2 m. For depth map, classes up to 10 m with 1 m interval were used. A last thematic class greater than 10 m was established since there was no occurrence of SAV beyond 10 m.

2.5. SAV Height Modeling

An analysis was performed to find out if the vegetation will grow less in low light, or if the plant will grow more in terms of height to reach sufficient radiation for its development, and also how the variations in both $K_{d(PAR)}$ and depth together influence the SAV height. Therefore, the sample points collected through the echosounder and the $K_{d(PAR)}$ estimated by the empirical model were combined, i.e., each sample point had $K_{d(PAR)}$ data, besides depth and SAV height data.

The digital model used in the present work was visualized with graphical resources usually used to characterize terrestrial surfaces such as temperature, altitude, etc. To produce this model,

it was necessary to interpolate the SAV height sample datasets as a function of $K_d(\text{PAR})$ and depth, instead of the usual X and Y coordinates. Thus, based on the presented solution, which is similar to a Digital Surface Model (DSM), it was possible to use the available surface reconstruction tools such as an inverse distance weighted (IDW) interpolation. The graphical representation was finally used to analyze the SAV height and distribution in a novel way. This graphical representation was elaborated to show how these three variables were related, so a visual analysis was performed to understand the phenomenon and also to estimate the height of SAV. The data were divided into five depth intervals for a better visualization: 0.5–2.0 m, 2.0–4.0 m, 4.0–6.0 m, 6.0–8.0 m and 8.0–10.0 m.

The SAV height as a function of depth and $K_d(\text{PAR})$ (independent variables) was represented as a DSM in which the domain of the function is given by the independent variables and the surface is produced by the IDW interpolation of the SAV height according to the values of this dependent variable. So, it was possible to observe the distribution of the SAV height as a function of $K_d(\text{PAR})$ and depth. Boolean expressions were created based on the model, creating a SAV height map based on $K_d(\text{PAR})$ and depth.

3. Results and Discussion

3.1. $K_d(\text{PAR})$ Mapping

$K_d(\text{PAR})$ was estimated using an empirical model based on R_{rs}^{SPOT} —predicted SPOT-6 bands [26]. $K_d(\text{PAR})$ regression presented higher accuracy using R_{rs}^{SPOT} (660 nm) with an R^2 of 92% (Figure 3a). Figure 3b shows the scatter plot between the measured and estimated $K_d(\text{PAR})$ based on SPOT image. Validation for $K_d(\text{PAR})$ showed a low bias (-0.09 m^{-1}) and an RMSE of 21.6%. The model based on the red band was then applied to the atmospherically corrected SPOT image to generate the map showing the spatial distribution of $K_d(\text{PAR})$ (Figure 4). In situ R_{rs} spectra acquired by RAMSES/TriOS sensors were predicted to match the SPOT-6 sensor bands and were compared with SPOT-6 atmospherically corrected sampling points for performance validation. More details of atmospheric correction of SPOT-6 in Rotta et al. [16] and Rotta et al. [26].

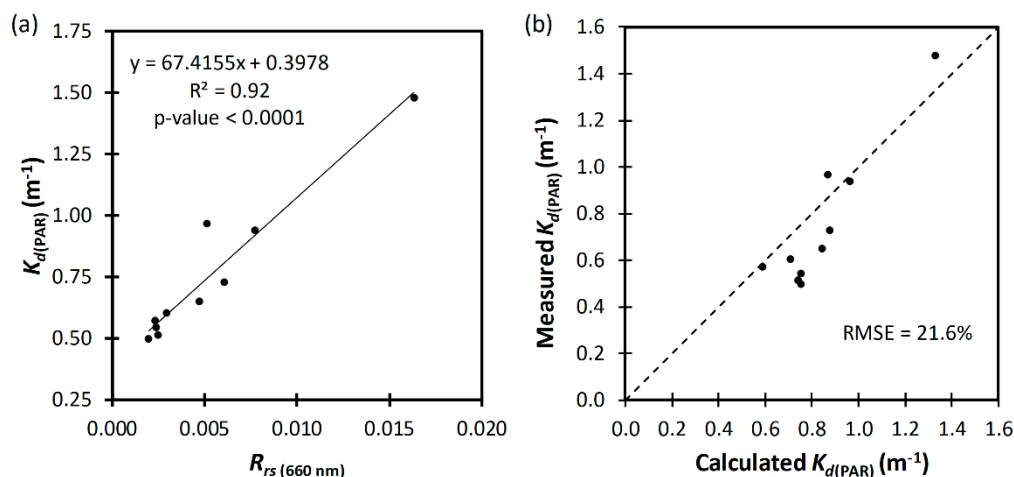


Figure 3. (a) The empirical model calibration based on the R_{rs}^{SPOT} —predicted SPOT band from R_{rs} measured in the field campaign. (b) validation based on the atmospherically corrected SPOT image.

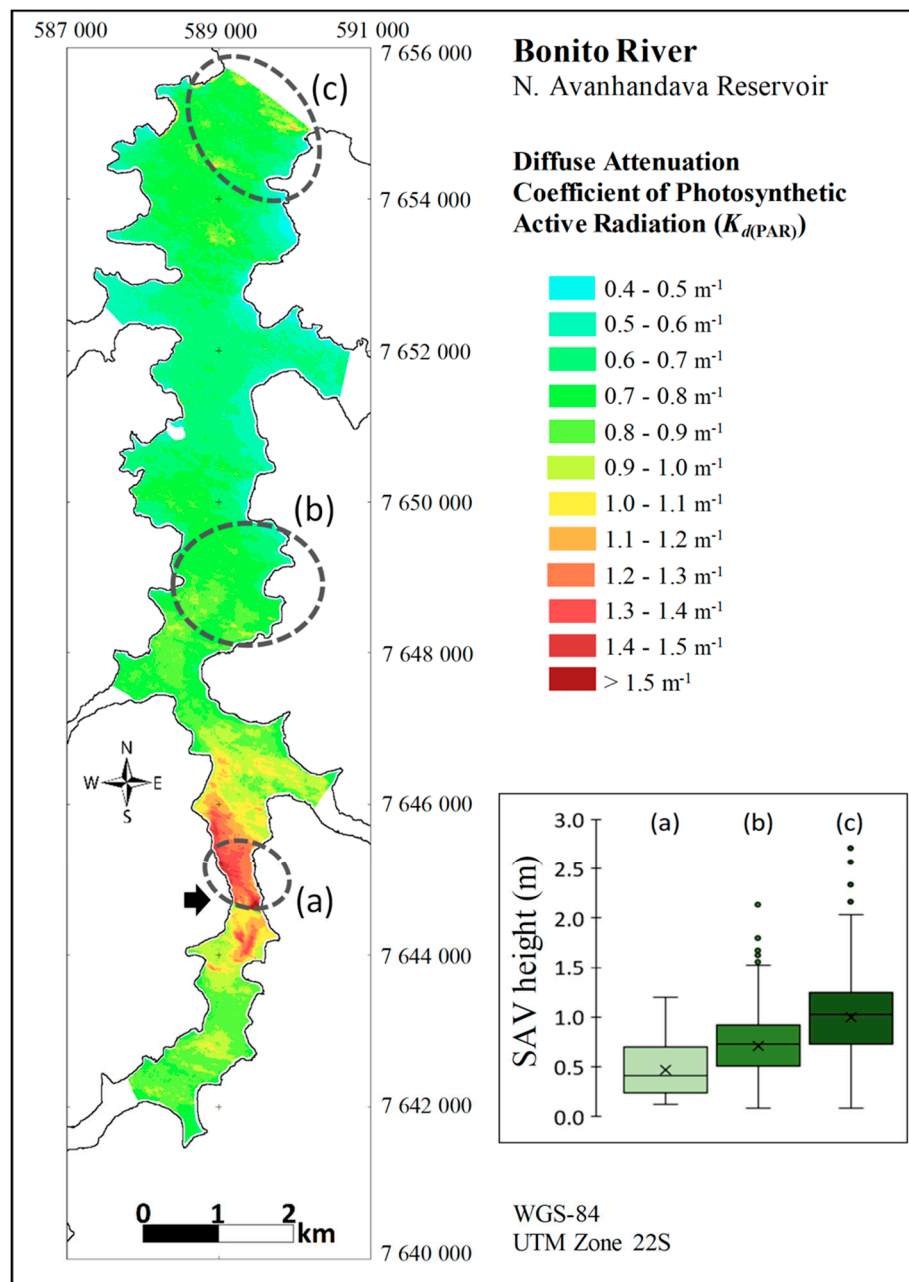


Figure 4. The $K_{d(PAR)}$ of Bonito River–Nova Avanhandava Reservoir. Boxplot of SAV height from the (a), (b) and (c) regions (dashed circles). The black arrow indicates a sand mining company location.

The spatial distribution of $K_{d(PAR)}$ was divided into 12 classes based on the minimum and maximum values. Lower values were observed in the downstream region of the study area, with values up to $1.0 m^{-1}$. Only 8% of the mapped area showed $K_{d(PAR)}$ greater than $1.0 m^{-1}$, and the majority of the area was represented by classes with $K_{d(PAR)}$ up to $1.0 m^{-1}$. The high transparency of the study area has favored the growth of submerged macrophytes.

Upstream areas are relatively shallow compared to the downstream areas, which could cause resuspension of bottom sediments induced by strong winds and water flow [1,48]. In downstream areas, the slow water flow due to the proximity of the dam and higher depths favored the deposition of suspended solids on the bottom, which resulted in a lower $K_{d(PAR)}$, as shown by Rotta et al. [15]. The region with a high $K_{d(PAR)}$ was observed near Figure 4a, and is probably caused by the presence of a sand mining company, indicated by the black arrow in Figure 4. Sand dredging leads to sediment resuspension that increased the K_d values at nearby locations [15]. Based on the $K_{d(PAR)}$ map, it can

be stated that most of these particles resuspended from the bottom were deposited again at locations approximately 2 km beyond the extraction point.

The region in Figure 4a is characterized by having higher values of $K_{d(PAR)}$ ($>1.2 \text{ m}^{-1}$), hence, this low transparency has interfered in SAV growth. This can be evidenced by the low values of SAV height shown in the boxplot (Figure 4). The boxplot was created from the echosounder dataset. A total of 600 sample points located inside each dashed circle were used in the plot. The regions in Figure 4b,c showed similar $K_{d(PAR)}$ values (between 0.4 and 1.0 m^{-1}), however, the SAV growth inside each region occurred in a different way, as evidenced by the box plot (Figure 4). In other words, the SAV in the region in Figure 4c is higher than that in the region in Figure 4b, even with similar $K_{d(PAR)}$ values. This proves that only $K_{d(PAR)}$ may not be sufficient to explain the distribution of SAV height in reservoirs. Caffrey et al. [6] suggest that light attenuation is the most important factor in determining the colonization depth of SAV, however, there is an important variability from one site to another, suggesting that other factors play a causal role in models to study SAV

3.2. Depth and SAV Height Mapping

3.2.1. Interpolation by Kriging

Based on the semivariograms, the pattern of spatial variability changed with the direction in both datasets (depth and SAV height), which confirms the anisotropy of the data. Different directions were tested for SAV height data and 70° was selected as the semivariogram with greater range (Figure 5a). It is worth mentioning that 90° is the north direction. The semivariogram of the perpendicular direction (160°) was plotted based on greater range direction (Figure 5b). The highest variance in the depth data was noted for direction 0° (Figure 5c); and the perpendicular direction was plotted in Figure 5d. The black dots represent the observed data and the gray lines are the fitted models.

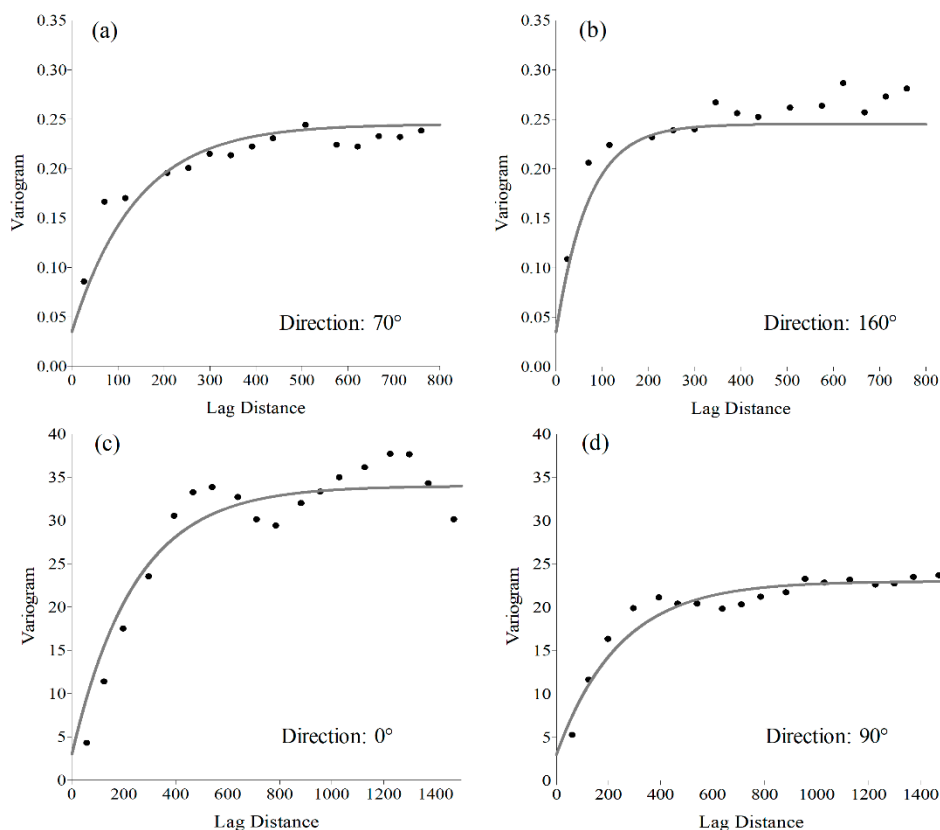


Figure 5. The semivariogram from SAV height data and exponential model for direction of greater range (a) 70° and (b) 160° (perpendicular direction). Semivariogram from depth data and exponential model for the direction of the greater sill (c) 0° and (d) 90° (perpendicular direction).

Geometric anisotropy was observed in semivariograms of SAV height data (Figure 5a,b), with a constant sill around 0.24, i.e., the variance of the data did not change with the direction. The greater range at 70° indicated the data interpolation in this direction should consider a larger distance. The model of the variogram was adjusted based on the exponential model (a scale of 0.21 and Length of 140 m), with a nugget effect of 0.035, an anisotropy ratio of 2 and an anisotropy angle of 70° (greater range). Zonal anisotropy was noted in semivariograms of depth data (Figure 5c,d), with the sill varying from 34 in direction of 0° to 23 in direction of 90°. The exponential model was selected with a Scale of 11 and 20, and Length of 240 m.

3.2.2. Depth and SAV Height Maps

The SAV height and water depth data acquired by the ecosounder were interpolated using ordinary kriging to generate their respective maps. Figure 6b shows the SAV height map in 12 classes, based on the minimum and maximum height observed in echosounder dataset. Figure 6a shows the depth map of the water body with 11 classes based on the maximum depth of occurrence of SAV observed in echosounder dataset. Although the SAV measured by echosounder have a high accuracy, as observed by Valey et al. [45], the dataset may contain errors related to the measurement procedure in the field. However, this error or measurement bias was not evaluated in this study because it was not possible to acquire in situ SAV height data manually.

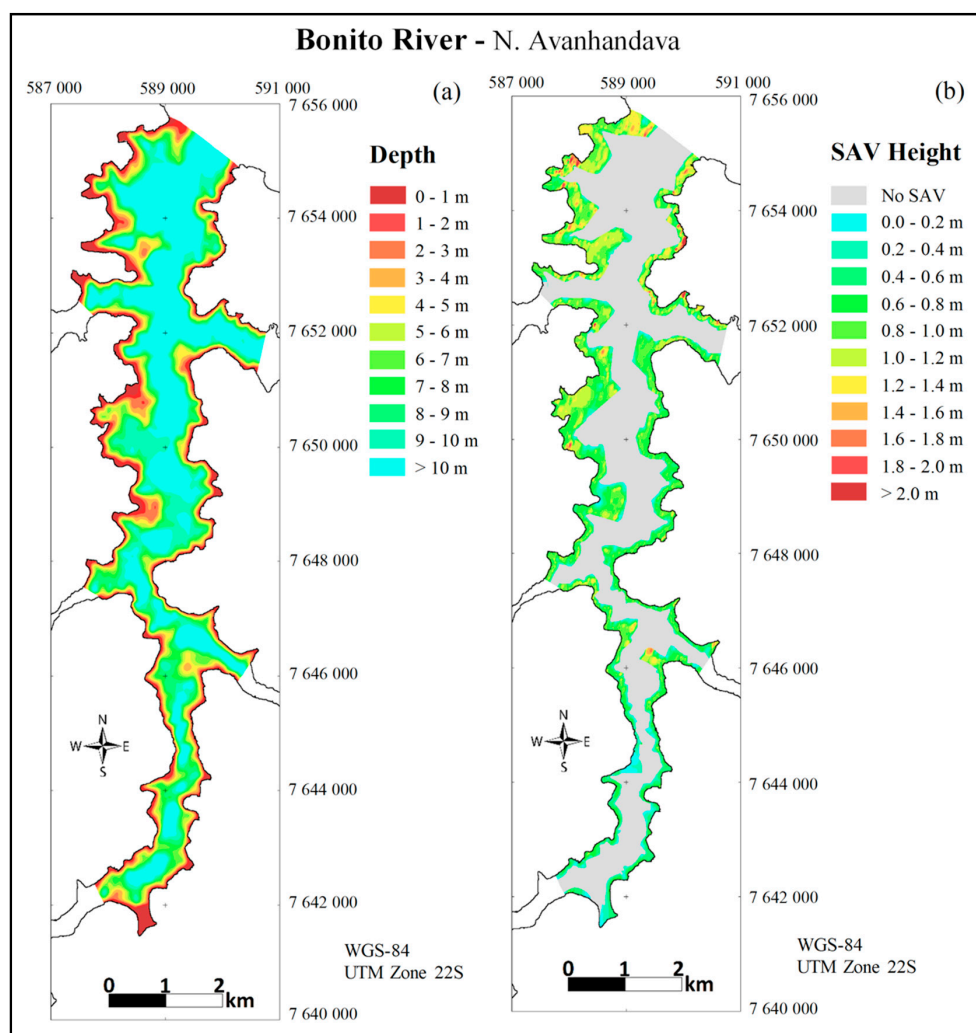


Figure 6. (a) The map of water depth and (b) map of submerged aquatic vegetation height, both based on interpolation by kriging.

In the upstream region, where the $K_{d(PAR)}$ values were higher (i.e., less transparency), the SAV height was smaller when compared with the downstream region. Thus, the transparency exerted a strong influence on SAV growth. In downstream, the majority of SAV height exhibited values around 1 m, with emphasis on small regions with SAV height close to 2 m. Besides $K_{d(PAR)}$, the depth of the water body may influence the SAV height, however, this hypothesis cannot be proved only with the depth map (Figure 6a). Therefore, a graphic based on the variables $K_{d(PAR)}$, depth and SAV height together can provide valuable information to analyze the SAV growth. The depth up to 30 m was measured in the study area, however, for the depth map, classes from 1 to 10 m and a class encompassing all depths above 10 m were considered. This is because the SAV presence was not recorded at depths beyond 10 m.

3.3. SAV Height Modeling

The scatterplot with the dataset of SAV height vs. depth, SAV height vs. $K_{d(PAR)}$ and $K_{d(PAR)}$ vs. depth is shown in Figure 7. Each point in the graphs represents the data of a sample point collected directly by the echosounder (SAV height and water body depth variables) or estimated by a calibrated model of $K_{d(PAR)}$ based on the satellite image.

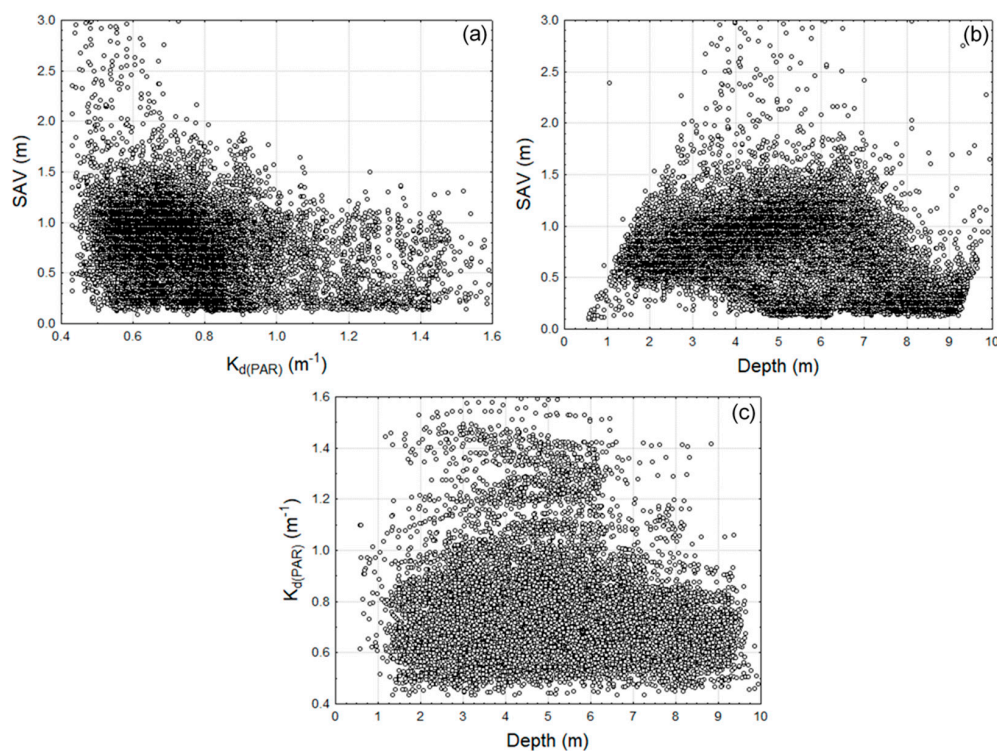


Figure 7. The scatterplot of SAV height vs. $K_{d(PAR)}$ (a), SAV height vs. depth (b) and $K_{d(PAR)}$ vs. depth (c).

Even though Figure 7 does not show clear cut evidence of the relationship between SAV vs. $K_{d(PAR)}$ (Figure 7a) and SAV vs. depth (Figure 7b), trends in both graphs were noted in the visual analysis. Lower $K_{d(PAR)}$ favors taller SAV in general. In depths smaller than 4 m, the SAV height is limited by a geometric constraint, in other words, the SAV cannot exceed the water column depth. Depths between 3 and 7 m provide a suitable environment macrophytes to grow taller. However, the $K_{d(PAR)}$ vs. depth (Figure 7c) did not show any significant correlation ($r = 0.097$). For depths greater than 7 m and $K_{d(PAR)}$ greater than $1 m^{-1}$, there were few sample points (Figure 7c) mainly because the SAV did not find conditions to grow. That means that at depths greater than 7 m, there must be an optimum transparency for the development of SAV. Therefore, given the difficulty in interpreting Figure 7 individually, a 3-D analysis using the three variables at the same time was performed.

Three-dimensional graphics based on the variables $K_d(\text{PAR})$, SAV height and depths are shown in Figure 8. The axes values for SAV height and $K_d(\text{PAR})$ were selected based on the minimum and maximum values in the dataset. In the depth axis, five different ranges were defined to have a better visualization of the SAV height behavior as a function of depth and $K_d(\text{PAR})$.

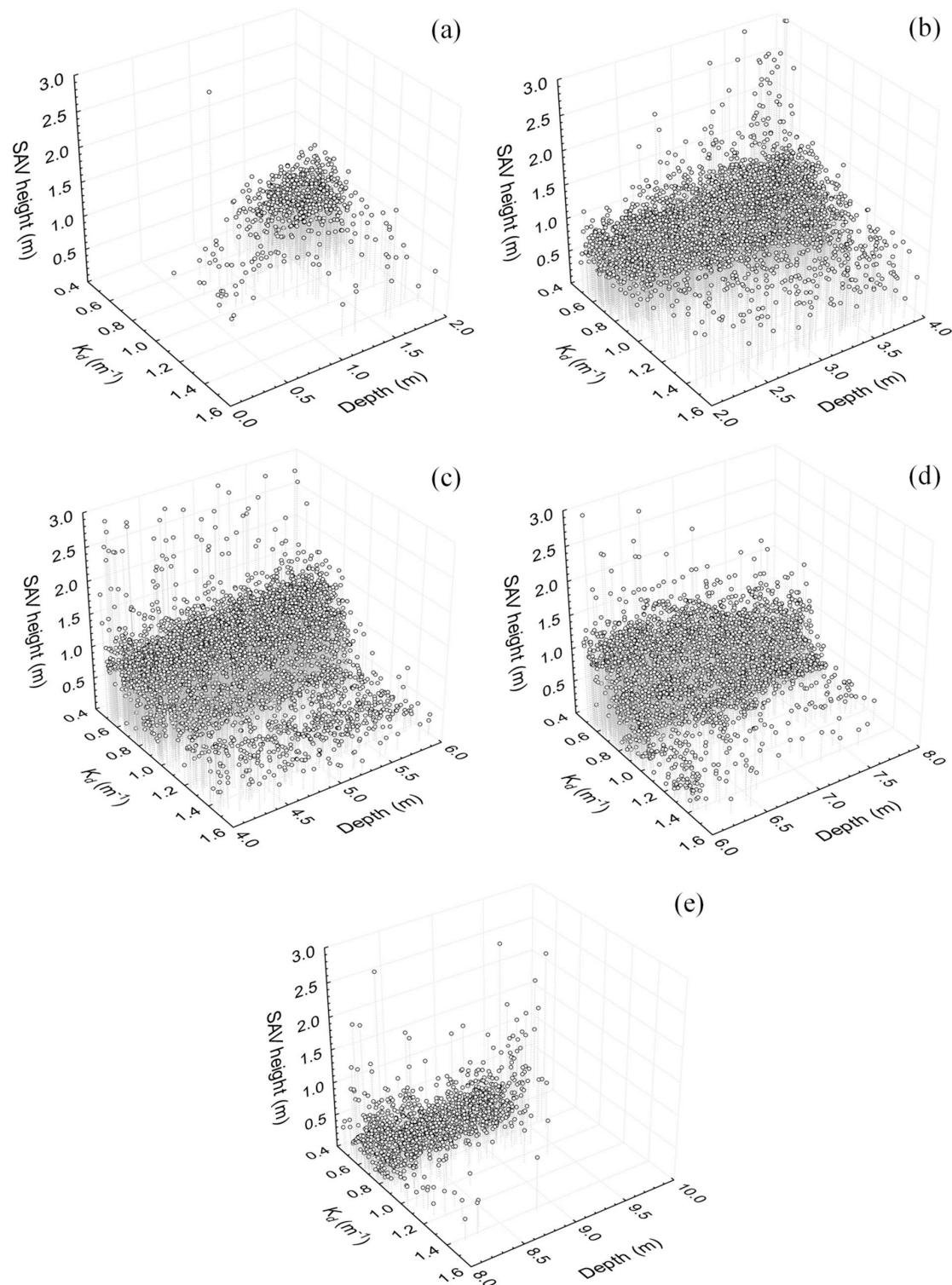


Figure 8. The three-dimensional graphics of dataset presenting SAV height vs. $K_d(\text{PAR})$ vs. Depth. (a) depth up to 2 m, (b) depth between 2 and 4 m, (c) depth between 4 and 6 m, (d) depth between 6 and 8 m, and (e) depth between 8 and 10 m.

Very short SAV values were found in depths up to 1 m. In general, for depths up to 2 m, the SAV height showed small variations even with the changing $K_{d(PAR)}$, i.e., the SAV height did not exceed 1 m. As shown by Rodrigues and Thomaz [13] and Tavechio and Thomaz [11], *Egeria densa* and *Egeria najas* (the main SAV found in Bonito River, Nova Avanhandava) require little radiation for their growth. The light compensation point of *E. najas* was reached between 6 and 22 $\mu\text{M m}^{-2} \text{s}^{-1}$ PAR by Tavechio and Thomaz [11] and between 7.5 and 16.2 $\mu\text{M m}^{-2} \text{s}^{-1}$ PAR for *E. densa* by Rodrigues and Thomaz [13]. The SAV are strongly influenced by excessive radiation in shallow waters. In addition, waves, variations in water level, and heavy runoff are common in these areas, increasing the likelihood of turbidity impairing the SAV growth as shown by Thomaz [12]. According to Vestergaard and Sand-Jensen [21], the growth of submerged macrophytes in large lakes may be restricted by wave action in shallow areas and light availability in deep areas.

In depths between 2 and 4 m, the maximum SAV height values had a slight increase with depth. In addition, taller SAV values occurred when $K_{d(PAR)}$ was minimal (close to 0.5 m^{-1}). There was no significant variation in the SAV height at depths from 3.5 to 7 m. In this depth range, the SAV height was mainly influenced by $K_{d(PAR)}$ responding inversely to it, in other words, the greater the transparency, the greater the SAV height at depths between 3.5 and 7 m. This behavior was also found in Bini and Thomaz [49], presenting an inverse relationship between the K_d and the probability of *E. najas* and *E. densa* occurrence in Itaipú Reservoir. At depths above 8 m, SAV occurred preferentially in waters with $K_{d(PAR)}$ lower than 1 m^{-1} . Caffrey et al. [6] showed that the maximum depth inhabited by a submerged macrophyte in Florida Lakes was 9.2 m in the lowest K_d value (about 0.2 m^{-1}).

Therefore, the existence and the height of SAV were directly influenced by the transparency ($K_{d(PAR)}$) of the water column, depending on the depth. Havens [10] showed SAV biomass-dependent to depth and transparency (based on TSS) in a shallow lake in Florida. The SAV growth could be favored if the water depth was maintained at less than 2 m and with a TSS below 20–30 mg L^{-1} [10]. However, the results did not clearly show whether or not SAV would reach high biomass under the favorable conditions [10].

The graphs in Figure 8 were not the most efficient way to identify how the SAV height depends on $K_{d(PAR)}$ and water depth. Therefore, the variables $K_{d(PAR)}$ and depth were considered as the XY axes and the variable SAV height as the Z axis in a three-dimensional graphic, and these variables were interpolated using the inverse distance weighting method (Figure 9). In other words, a digital model of SAV height based on $K_{d(PAR)}$ and depth was created. The values of each axis are related with the minimum and maximum of each variable. Based on this model, it was possible to analyze the behavior of the SAV height from the combination of the depth and $K_{d(PAR)}$ variables.

In regions with depths between 1 and 4 m and up to the maximum $K_{d(PAR)}$ value of the studied area (around 1.6 m^{-1}), the SAV was well-developed, with height about 1 m. In these regions, the SAV growth was favored because there is enough radiation in that depth range. At depths between 4 and 6 m, high values of SAV height (about 1.5 m) were observed only when $K_{d(PAR)}$ was low ($0.4\text{--}0.7 \text{ m}^{-1}$), which indicates that in this depth range, the SAV growth is strongly influenced by the water transparency (or K_d). Taller SAV, up to around 2 m height occurred at depths from 3.5 to 7 m and in $K_{d(PAR)}$ up to 0.5 m^{-1} , in other words, the SAV were well-developed in this depth range as long as the $K_{d(PAR)}$ remained low (lower than 0.5 m^{-1}). Canfield Jr. et al. [50] showed a significant positive relationship ($r = 0.70$) between the maximum depth of the macrophyte colonization (Z_{max}) and transparency (based on the Secchi depth). A negative relationship between Z_{max} and the attenuation coefficient was verified by Canfield Jr. et al. [50], and their model presented $R^2 = 0.41$. Thereby, both the SAV height and the maximum depth of the macrophyte colonization (Z_{max}) seem to be strongly influenced by water transparency.

In deeper regions and with significantly high $K_{d(PAR)}$, the SAV can stretch themselves to survive. This behavior of elongation in *Egeria* is described by Tavechio and Thomaz [11] and Rodrigues and Thomaz [13]. This elongation does not necessarily mean a growth in biomass since it could not have sufficient radiation for photosynthesis. It is only a survival mechanism of the species present in the

study area (*E. densa* and *E. najas*). However, above a given $K_d(\text{PAR})$ (a maximum of 1.6 m^{-1} in our studied area) or depth (about 10 m), the SAV were not able to grow in Nova Avanhandava Reservoir. There were few samples of SAV in areas with depths greater than 9 m. However, their development is quite limited in this region mainly because of the insufficient radiation and high pressure. In deep regions, the SAV just developed under high transparency conditions, i.e., low $K_d(\text{PAR})$. According to Wetzel [1] submerged macrophytes can occur at all depths within the euphotic zone, however, vascular angiosperms (such as *Egeria* spp.) occur only at about 10 m due to the hydrostatic pressure.

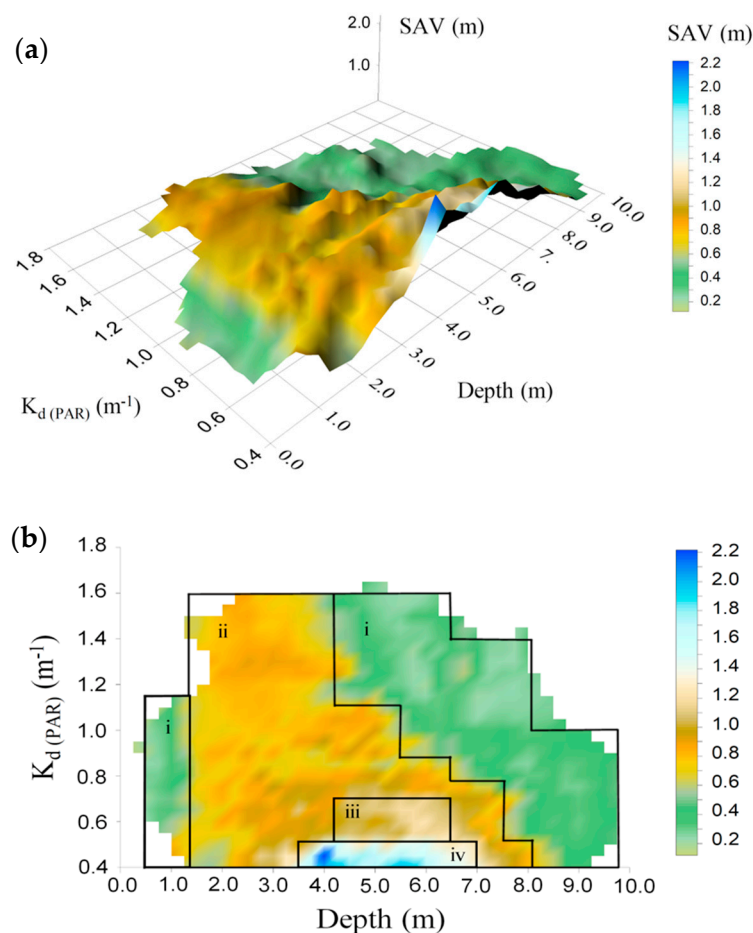


Figure 9. The digital model represented by a three-dimensional graphic of SAV height vs. $K_d(\text{PAR})$ vs. Depth interpolated by inverse distance weighting in (a). Digital model of $K_d(\text{PAR})$ vs. Depth in (b) divided into four classes based on the SAV height: i = low, ii = medium, iii = high and iv = very high.

Using the Figure 9b the SAV heights were divided into four classes: i = low, ii = medium, iii = high and iv = very high. Boolean expressions based on $K_d(\text{PAR})$ and depth values were developed to classify the four SAV height classes. It should be noted that $K_d(\text{PAR})$ data were estimated by the $K_d(\text{PAR})$ model applied to the SPOT-6 image and the depth data were based on echosounder data interpolated by kriging. Figure 10 shows the SAV map based on the Boolean expressions.

This kind of classification (Figure 10) would not be possible without generating a digital model based on the K_d and depth. Based on this model it was possible to create the spatial distribution (latitude, longitude) of the SAV height classes. The “High” and “Very high” classes were just found at downstream region because of their lower $K_d(\text{PAR})$. “Medium” and “Low” classes were identified along with the whole water body since these classes occurred in a wide range of $K_d(\text{PAR})$ (between 0.4 and 1.6) and depth (up to about 10 m). It is worth mentioning that the regions classified as “Low” SAV height had the necessary conditions for the development of SAV (although limited), however, some of that regions could not actually have SAV at the time of field survey.

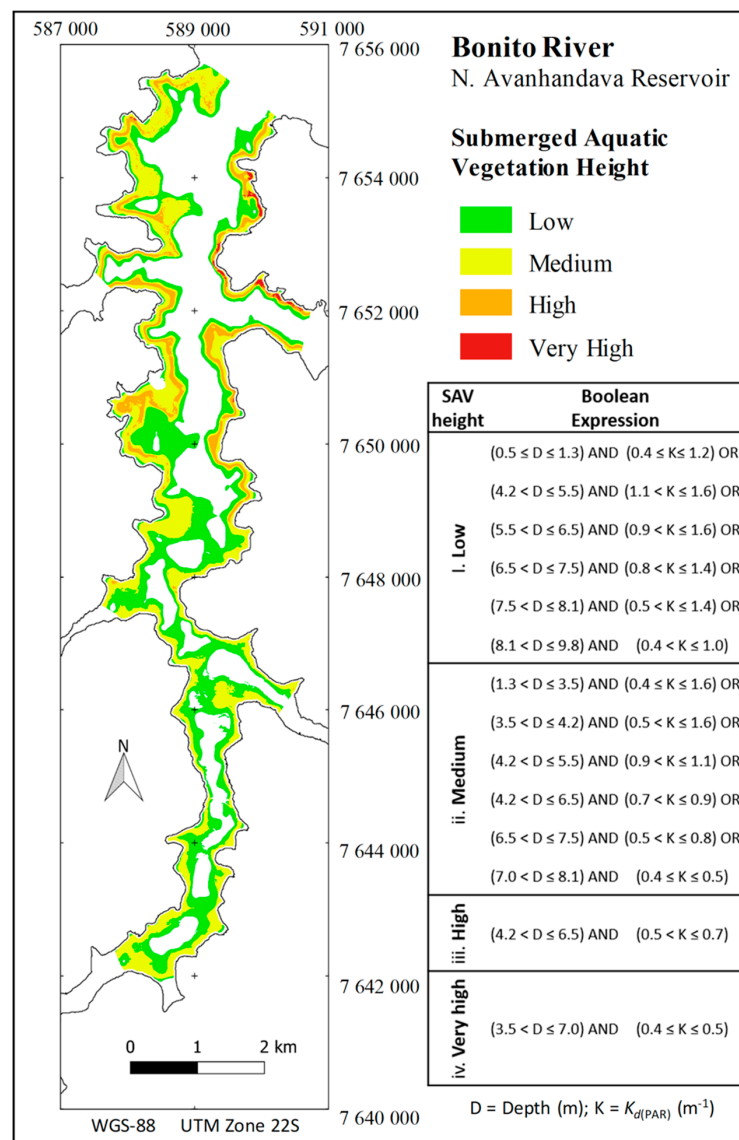


Figure 10. The SAV height map classified with Boolean expressions based on depth and $K_{d(PAR)}$. The Boolean expressions are shown in the table.

Estimating the SAV height based on just transparency (or K_d) may not be enough since the development of SAV is directly influenced by the water column depth. The proposed methodology of a digital model based on $K_{d(PAR)}$ and depth to estimate the SAV height classes was novel and presented wide contribution in SAV studies. In addition, other factors may exert influence, even if small, on the growth of SAV. Canfield Jr. et al. [50] calculated a model to predict Z_{max} based on the Secchi depth. Their model tends to underestimate the result in very clear water and overestimate it when the Secchi depth is low ($R^2 = 0.56$). They indicate that improvements in the model estimative will occur only when the factors contributing to the variability in Z_{max} are well understood [50]. According to Caffrey et al. [6], the macrophyte species, sediment type and slope can influence the aquatic plant colonization in an individual lake, however, these factors did not increase the predictive capability of their model to estimate Z_{max} based on the Secchi depth. Canfield Jr. et al. [50] indicate that improvements in the model estimative will occur only when one understands which factors contribute to the variability in the maximum depth of macrophyte colonization. Therefore, a $K_{d(PAR)}$ and depth based model can contribute to a better understanding of presence and height distribution of aquatic macrophytes in reservoirs.

4. Conclusions

The $K_d(\text{PAR})$ estimated from an empirical model based on predicted SPOT-6 bands and applied to atmospherically corrected SPOT-6 image presented R^2 of 92% and RMSE of 21.6%. The kriging generated from the echosounder data (SAV height and depth) provided spatial distribution maps for each variable. Anisotropy was observed in semivariograms of SAV height and depth data. Based on the downstream of SAV height map, most values around 1 m and small regions with 2 m were observed. The depth of the water body can influence the SAV growth too. Depth classes from 1 to 10 m in the map were considered since the SAV in the studied area occur only at depths less than about 10 m due to the hydrostatic pressure and radiation needed. When comparing the $K_d(\text{PAR})$ and the SAV height maps, a trend in the spatial distribution of these variables was noted. In the regions with higher $K_d(\text{PAR})$ (upstream), there were shorter SAV, and in the regions with lower $K_d(\text{PAR})$ (downstream), maximum SAV heights were observed. However, it was difficult to assess the SAV height distribution only using individual $K_d(\text{PAR})$ and depth maps.

The digital model and mainly its graphical representation were used to analyze how the SAV responds to the independent variables, depth and $K_d(\text{PAR})$, in the studied region. It was concluded that the model overcomes the limitations found by other researchers in understanding the SAV behavior in relation to those independent variables. Based on visual analysis of the model ($K_d(\text{PAR})$ vs. depth vs. SAV height) it was possible to identify the relationships between the variables that could have been difficult to achieve without this approach. The results have shown to be promising and the proposed methodology can help to understand the SAV dynamics in reservoirs in a simpler and faster way. However, the results were supported by a limited dataset, i.e., data from a single field survey and a single reservoir. Therefore, the impact of variations in the concentrations of optically active constituents (e.g., Chl-a, TSS, CDOM) in the water or growth stages of vegetation on the SAV height model's accuracy needs to be further evaluated. Additionally, multi-temporal satellite data could be used in the further analysis of SAV height distribution in reservoirs, however, they would most likely pose additional complications arising from temporal differences in atmospheric scattering and need to be incorporated in the SAV height model to make it scalable and robust. This could form a part of the future study where the impact of water quality and vegetation phenology on the SAV model output can be examined.

Just a few plants were found at depths up to 1 m and in these few specimens; the SAV heights were very short. In very shallow waters, the SAV can be negatively influenced by excess radiation [11,13] and by waves action and variation in water level [12,21]. The SAV height values had a slight increase at depths from 2 to 4 m, with taller SAV occurring in low $K_d(\text{PAR})$ (0.5 m^{-1}) areas. At depths between 4 and 6 m, the SAV height was strongly influenced by $K_d(\text{PAR})$, where high values of SAV height (about 1.5 m) were observed only when $K_d(\text{PAR})$ was low ($0.4\text{--}0.7 \text{ m}^{-1}$). The tallest SAV occurred at depths from 3.5 to 7 m and $K_d(\text{PAR})$ up to 0.5 m^{-1} , i.e., SAV were well-developed (up to 2 m) in this depth range as long as the $K_d(\text{PAR})$ remained low. There were few SAV growing at depths greater than 9 m and they were totally extinct after 10 m due to insufficient radiation and high pressure.

It was observed that the SAV height classes based on $K_d(\text{PAR})$ and depth had a well-defined behavior in the studied reservoir. Thus, based on the visual analysis it was possible to establish a set of Boolean rules to classify the SAV height and identify regions where SAV can grow with greater or lesser vigor. So, the studied area was classified producing a spatial distribution representation of SAV height classes. The "High" and "Very high" classes were just found at the downstream region because of their lower $K_d(\text{PAR})$. "Medium" and "Low" classes were identified along the whole water body since these classes occurred in a wide range of $K_d(\text{PAR})$ and depth. The regions classified as "Low" SAV height had limited conditions for its growth, so those regions could not actually have SAV at the time of the field survey. Estimating the SAV height based on just transparency (or K_d) cannot be enough since the development of SAV is directly influenced by the water column depth. The proposed methodology of a digital model based on $K_d(\text{PAR})$ and depth to estimate SAV height classes was novel and presented a wide contribution in SAV studies. This methodology for monitoring SAV should

be tested in other reservoirs or freshwater lakes to better understand the relationship between SAV characteristics, and $K_d(\text{PAR})$ and depth. For this, $K_d(\text{PAR})$ and water depth data from a new field survey could be used to either tune or validate the model for SAV height estimation by comparing the results obtained in this study. Ultimately, the model could be useful in efforts to monitor and control SAV based on bathymetry and water body transparency (or K_d).

The $K_d(\text{PAR})$ can indicate the radiation availability for SAV at a given depth. Variation in $K_d(\text{PAR})$ at a constant depth generate different conditions of radiation availability. Variation in depth but keeping the $K_d(\text{PAR})$ value can also create different conditions of radiation availability. It is known that radiation availability acts as the main limiting factor for SAV growth, however, the importance of studying SAV based on both transparency and depth variables can be evidenced in this study. In future, samples from other regions with a wide variety of optical properties could be incorporated into the model to create a robust version which can be applied to the entire reservoir and to others similar aquatic environments.

It should be noted that the SAV height field survey is extremely time consuming and labor intensive and, therefore, studies using SAV height data tend to be scarce. This study presented the initial results of a proposed methodology, which is based mainly on visual analysis. It is noteworthy that the model was developed in an oligotrophic reservoir, and its applicability in different environments has not been tested yet. We intend to conduct a new and independent field survey to further evaluate the results and ultimately add more data and more sites to make the model more scalable.

Author Contributions: L.H.R., F.W. and T.R. carried out field surveys and did laboratorial analysis. E.A. and N.I. managed the projects that funded the dataset acquisition in field campaign and data processing. D.R.M., E.A. and N.I. supervised the first author in Doctoral and Postdoc studies. L.H.R. conducted the experiments and wrote the paper. All authors reviewed and edited the manuscript.

Funding: This research was funded by São Paulo Research Foundation—FAPESP, grant number 2012/19821-1, 2013/09045-7 and 15/21586-9 and National Counsel of Technological and Scientific Development-CNPq, grant number 400881/2013-6, 472131/2012-5 and 482605/2013-8.

Acknowledgments: The authors wish to thank the FAPESP and the CNPq for financial support and PNPd/CAPES for scholarship. Thanks to the University of Georgia (UGA) for facilitating collaboration between UNESP and UGA through the international student exchange program.

Conflicts of Interest: The authors declare no conflict of interest.

References

1. Wetzel, R.G. *Limnology: Lake and River Ecosystems*, 3rd ed.; Academic Press: San Diego, CA, USA, 2001.
2. Tundisi, J.G.; Matsumura-Tundisi, T. *Limnologia*; Oficina de Textos: São Paulo, Brazil, 2008.
3. Thomaz, S.M.; Esteves, F.A.; Murphy, K.J.; Dos-Santas, A.M.; Caliman, A.; Guariento, R.D. Aquatic Macrophytes in the Tropics: Ecology of Population and Communities, Impact of Invasion and Use by Man. In *Tropical Biology and Conservation Management: Ecology*; Del Claro, K., Oliveira, P.S., Rico-Gray, V., Eds.; EOLSS/UNESCO: Oxford, UK, 2008; Volume V.
4. Jakubauskas, M.E.; Peterson, D.L.; Campbell, S.W.; de Noyelles, F., Jr.; Campbell, S.D.; Penny, D. Mapping and Monitoring Invasive Aquatic Plant Obstructions in Navigable Waterways Using Satellite Multispectral Imagery. In Proceedings of the Pecora 15/Land Satellite Information IV/ISPRS Commission I/FIEOS 2002 Conference, Denver, CO, USA, 10–15 November 2002.
5. Rockwell, H.W. *Summary of a Survey of the Literature on the Economic Impact of Aquatic Weeds. The Economic Impact of Aquatic Weed*; Report for the Aquatic Ecosystem Restoration Foundation; Aquatic Ecosystem Restoration Foundation: Marietta, GA, USA, 2003. Available online: http://www.aquatics.org/pubs/economic_impact.pdf (accessed on 5 November 2018).
6. Caffrey, A.J.; Hoyer, M.V.; Canfield, D.E., Jr. Factors Affecting the Maximum Depth of Colonization by Submersed Macrophytes in Florida Lakes. *Lake Reserv. Manag.* **2007**, *23*, 287–297. [CrossRef]
7. Camargo, A.F.M.; Pezzato, M.M.; Henry-Silva, G.G. Limitant Factors to Primary Production of Aquatic Macrophytes, “Fatores Limitantes à Produção Primária Macrófitas Aquáticas”. In *Ecologia e Manejo de Macrófitas Aquáticas*; Thomaz, S.M., Bini, L.M., Eds.; EDUEM: Maringá, Brazil, 2003; pp. 59–83.

8. Biudes, J.F.V.; Camargo, A.F.M. Studying the Limiting Factors to Primary Production of Aquatic Macrophytes in Brazil. *Oecol. Bras.* **2008**, *12*, 7–19. [[CrossRef](#)]
9. Schwarz, A.M.; Wintonb, M.; Hawes, I. Species-Specific Depth Zonation in New Zealand Charophytes as a Function of Light Availability. *Aquat. Bot.* **2002**, *72*, 209–217. [[CrossRef](#)]
10. Havens, K.E. Submerged aquatic vegetation correlations with depth and light attenuating materials in a shallow subtropical lake. *Hydrobiologia* **2003**, *493*, 173–186. [[CrossRef](#)]
11. Tavechio, W.L.G.; Thomaz, S.M. Effects of Light on the Growth and Photosynthesis of *Egeria najas* Planchon. *Braz. Arch. Biol. Technol.* **2003**, *46*, 203–209. [[CrossRef](#)]
12. Thomaz, S.M. Fatores que Afetam a Distribuição e o Desenvolvimento de Macrófitas Aquáticas em Reservatórios: Uma Análise em Diferentes Escalas. In *Ecologia de Reservatórios: Impactos Potenciais, Ações de Manejo e Sistemas em Cascata*; Nogueira, M.G., Henry, R., Jorcin, A., Eds.; RiMa: São Carlos, Brazil, 2006; pp. 165–181.
13. Rodrigues, R.B.; Thomaz, S.M. Photosynthetic and Growth Responses of *Egeria Densa* to Photosynthetic Active Radiation. *Aquat. Bot.* **2010**, *92*, 281–284. [[CrossRef](#)]
14. Kirk, J.T.O. *Light and Photosynthesis in Aquatic Ecosystems*, 3rd ed.; Cambridge University Press: New York, NY, USA, 2011.
15. Rotta, L.H.S.; Mishra, D.R.; Alcântara, E.H.; Imai, N.N. Analyzing the status of submerged aquatic vegetation using novel optical parameters. *Int. J. Remote Sens.* **2016**, *37*, 3786–3810. [[CrossRef](#)]
16. Rotta, L.H.S.; Mishra, D.R.; Watanabe, F.S.Y.; Rodrigues, T.W.P.; Alcântara, E.H.; Imai, N.N. Analyzing the feasibility of a space-borne sensor (SPOT-6) to estimate the height of submerged aquatic vegetation (SAV) in inland waters. *ISPRS J. Photogramm. Remote Sens.* **2018**, *144*, 341–356. [[CrossRef](#)]
17. Gallegos, C.L. Calculating Optical Water Quality Targets to Restore and Protect Submersed Aquatic Vegetation: Overcoming Problems in Partitioning the Diffuse Attenuation Coefficient for Photosynthetically Active Radiation. *Estuaries* **2001**, *24*, 381–397. [[CrossRef](#)]
18. Mishra, D.R.; Narumalani, S.; Rundquist, D.; Lawson, M. Charactering the Vertical Diffuse Attenuation Coefficient for Downwelling Irradiance in Coastal Waters: Implications for Water Penetration by High Resolution Satellite Data. *ISPRS J. Photogramm. Remote Sens.* **2005**, *60*, 48–64. [[CrossRef](#)]
19. Mishra, D.R.; Narumalani, S.; Rundquist, D.; Lawson, M.; Perk, R. Enhancing the detection and classification of coral reef and associated benthic habitats: A hyperspectral remote sensing approach. *J. Geophys. Res.* **2007**, *112*, C08014. [[CrossRef](#)]
20. Hudon, C.; Lalonde, S.; Gagnon, P. Ranking the effects of site exposure, plant growth form, water depth, and transparency on aquatic plant biomass. *Can. J. Fish. Aquat. Sci.* **2000**, *57* (Suppl. 1), 31–42. [[CrossRef](#)]
21. Vestergaard, O.; Sand-Jensen, K. Aquatic macrophyte richness in Danish lakes in relation to alkalinity, transparency, and lake area. *Can. J. Fish. Aquat. Sci.* **2000**, *57*, 2022–2031. [[CrossRef](#)]
22. Nielsen, S.L.; Sand-Jensen, K.; Borum, J.; Geertz-Hansen, O. Depth Colonization of Eelgrass (*Zostera marina*) and Macroalgae as Determined by Water Transparency in Danish Coastal Waters. *Estuaries* **2002**, *25*, 1025–1032. [[CrossRef](#)]
23. Rodrigues, T.W.P.; Alcântara, E.H.; Mishra, D.R.; Watanabe, F.S.Y.; Bernardo, N.M.R.; Rotta, L.H.S.; Imai, N.N.; Astuti, I. Performance of existing QAAs in Secchi disk depth retrieval in phytoplankton and dissolved organic matter dominated inland waters. *J. Appl. Remote Sens.* **2018**, *12*, 036017. [[CrossRef](#)]
24. Rodrigues, T.W.P.; Alcantara, E.H.; Watanabe, F.S.Y.; Imai, N.N. Retrieval of Secchi disk depth from a reservoir using a semi-analytical scheme. *Remote Sens. Environ.* **2017**, *198*, 213–228. [[CrossRef](#)]
25. Watanabe, F.S.Y.; Mishra, D.R.; Astuti, I.; Rodrigues, T.W.P.; Alcantara, E.H.; Imai, N.N.; Barbosa, C.C.F. Parametrization and calibration of a quasi-analytical algorithm for tropical eutrophic Waters. *ISPRS J. Photogramm. Remote Sens.* **2016**, *121*, 28–47. [[CrossRef](#)]
26. Rotta, L.H.S.; Alcântara, E.H.; Watanabe, F.S.Y.; Rodrigues, T.W.P.; Imai, N.N. Atmospheric correction assessment of SPOT-6 image and its influence on models to estimate water column transparency in tropical reservoir. *Remote Sens. Appl. Soc. Environ.* **2016**, *4*, 158–166. [[CrossRef](#)]
27. SSRH/CRHi. *Situação dos Recursos Hídricos no Estado de São Paulo*; Ano base 2009; Secretaria de Saneamento e Recursos Hídricos, Coordenadoria de Recursos Hídricos: São Paulo, Brazil, 2011. Available online: http://www.sigrh.sp.gov.br/sigrh/basecon/RelatorioSituacao2011/Relatorio_Situacao_2011.pdf (accessed on 8 May 2013).

28. Petesse, M.L.; Petrere, M., Jr. Tendency towards homogenization in fish assemblages in the cascade reservoir system of the Tietê river basin, Brazil. *Ecol. Eng.* **2012**, *48*, 109–116. [\[CrossRef\]](#)
29. Cavenaghi, A.L.; Velini, E.D.; Galo, M.L.B.T.; Carvalho, F.T.; Negrisoni, E.; Trindade, M.L.B.; Simionato, J.L.A. Characterization of Water Quality and Sediment Related to the Occurrence of Aquatic Plants in Five Tietê Waterhed Reservoirs. “Caracterização da Qualidade de Água e Sedimento Relacionados com a Ocorrência de Plantas Aquáticas em Cinco Reservatórios da Bacia do Rio Tietê”. *Planta Daninha* **2003**, *21*, 43–52. [\[CrossRef\]](#)
30. Velini, E.D.; Galo, M.L.B.T.; Carvalho, F.T.; Martins, D.; Cavenaghi, A.L.; Trindade, M.L.B.; Bravin, L.F.B.; Negrisoni, E.; Antuniassi, U.R.; Simionato, J.L.A.; et al. Assessment of Aquatic Plants in the Reservoirs of AES-Tietê and Development of an Integrated Control Model for the Most Important Species. *J. Environ. Sci. Health* **2005**, *40*, 85–100. [\[CrossRef\]](#)
31. Dall’olmo, G.; Gitelson, A.A. Effect of Bio-Optical Parameter Variability on the Remote Estimation of Chlorophyll-A Concentration in Turbid Productive Waters: Experimental Results. *Appl. Opt.* **2005**, *44*, 412–422. [\[CrossRef\]](#) [\[PubMed\]](#)
32. Gitelson, A.A.; Dall’olmo, G.; Moses, W.; Rundquist, D.C.; Barrow, T.; Fisher, T.R.; Gurlin, D.; Holz, J. A Simple Semi-Analytical Model for Remote Estimation of Chlorophyll-A in Turbid Waters: Validation. *Remote Sens. Environ.* **2008**, *112*, 3582–3593. [\[CrossRef\]](#)
33. Astrum. *Spot 6 & Spot 7 Imagery—User Guide*; Si/Dc/13034-V1.0; Astrum: Toulouse, France, 2013; pp. 1–120.
34. Mobley, C.D. *Light and Water: Radiative Transfer in Natural Waters*; Academic Press: San Diego, CA, USA, 1994.
35. Biosonics. *User Guide: BioSonics X-Series Echosounder and Visual Acquisition 5.0*; Biosonics Inc.: Seattle, WA, USA, 2002; pp. 1–60.
36. Biosonics. *User Guide: EcoSAV 1*; Biosonics Inc.: Seattle, WA, USA, 2008; pp. 1–48.
37. Biosonics. *Calibration of BioSonics Digital Scientific Echosounder Using T/C Calibration Spheres*; Biosonics Inc.: Seattle, WA, USA, 2004; pp. 1–11.
38. Sabol, B.M.; Melton, R.E.; Chamberlan, R.; Doering, P.; Haunert, K. Evaluation of A Digital Echo Sounder System for Detection of Submersed Aquatic Vegetation. *Estuaries* **2002**, *25*, 133–141. [\[CrossRef\]](#)
39. Chamberlain, R.H.; Doening, P.H.; Orlando, B.; Sabol, B.M. Comparison of Manual and Hydroacoustic Measurement of Seagrass Distribution in the Caloosahatchee Estuary, Florida. *Fla. Sci.* **2009**, *72*, 386–405.
40. Stone, M. Cross-Validatory Choice and Assessment of Statistical Predictions. *J. R. Stat. Soc. Ser. B (Methodol.)* **1974**, *36*, 111–147. [\[CrossRef\]](#)
41. Arlot, S.; Celisse, A. A survey of cross-validation procedures for model selection. *Stat. Surv.* **2010**, *4*, 40–79. [\[CrossRef\]](#)
42. Adler-Golden, S.M.; Matthew, M.W.; Bernstein, L.S.; Levine, R.Y.; Berk, A.; Richtsmeier, S.C.; Acharya, P.K.; Anderson, G.P.; Felde, G.; Gardner, J.; et al. Atmospheric correction for shortwave spectral imagery based on MODTRAN4. SPIE Proc. Imaging Spectrom. *Proc. SPIE* **1999**, *3753*, 61–69. [\[CrossRef\]](#)
43. Yamamoto, J.K.; Landim, P.M.B. *Geoestatística: Conceitos e aplicações*; Oficina de Textos: São Paulo, Brazil, 2013.
44. Rotta, L.H.S. Inferência Espacial Para Mapeamento de Macrófitas Submersas—Estudo de Caso. Dissertation of Master’s Degree—Cartographic Sciences, São Paulo State University, São Paulo, Brazil, 2011. Available online: http://www2.fct.unesp.br/pos/cartografia/docs/teses/d_rotta_lh.pdf (accessed on 5 November 2018).
45. Valley, R.D.; Drake, M.T.; Anderson, C.S. Evaluation of alternative interpolation techniques for the mapping of remotely-sensed submersed vegetation abundance. *Aquat. Bot.* **2005**, *81*, 13–25. [\[CrossRef\]](#)
46. Goovaerts, P. *Geostatistics for Natural Resources Evaluation*; Oxford University Press: New York, NY, USA, 1997.
47. Isaaks, E.H.; Srivastava, R.M. *An Introduction to Applied Geostatistics*; Oxford University Press: New York, NY, USA, 1989.
48. Cho, H.J. Effects of Prevailing Winds on Turbidity of a Shallow Estuary. *Int. J. Environ. Res. Public Health* **2007**, *4*, 185–192. [\[CrossRef\]](#)
49. Bini, L.M.; Thomaz, S.M. Prediction of *Egeria najas* and *Egeria densa* occurrence in a large subtropical reservoir (Itaipu Reservoir, Brazil-Paraguay). *Aquat. Bot.* **2005**, *83*, 227–238. [\[CrossRef\]](#)
50. Canfield, D.E., Jr.; Langeland, K.A.; Lind, S.B.; Haller, W.T. Relations between water transparency and maximum depth of macrophyte colonization in lakes. *J. Aquat. Plant Manag.* **1985**, *23*, 25–28.

